BASIC RESEARCH www.jasn.org

Megalin-Mediated Tubuloglomerular Alterations in High-Fat Diet–Induced Kidney Disease

Shoji Kuwahara,* Michihiro Hosojima,† Reika Kaneko,* Hiroyuki Aoki,* Daisuke Nakano,‡ Taiji Sasagawa,§ Hideyuki Kabasawa,§ Ryohei Kaseda,† Ryota Yasukawa,§ Tomomi Ishikawa,§ Akiyo Suzuki,§ Hiroyoshi Sato,* Shun Kageyama,‖ Takahiro Tanaka,¶ Nobutaka Kitamura,¶ Ichiei Narita,§ Masaaki Komatsu,‖ Akira Nishiyama,‡ and Akihiko Saito*

*Department of Applied Molecular Medicine, †Department of Clinical Nutrition Science, §Division of Clinical Nephrology and Rheumatology, and ‖Department of Biochemistry, Niigata University Graduate School of Medical and Dental Sciences, Niigata, Japan; ‡Department of Pharmacology, Faculty of Medicine, Kagawa University, Kagawa, Japan; and ¶Protocol Data Center, Niigata University Medical and Dental Hospital, Niigata, Japan

ABSTRACT

Obesity, an important risk factor for metabolic syndrome (MetS) and cardiovascular disease, is often complicated by CKD, which further increases cardiovascular risk and causes ESRD. To elucidate the mechanism underlying this relationship, we investigated the role of the endocytic receptor megalin in proximal tubule epithelial cells (PTECs). We studied a high-fat diet (HFD)–induced obesity/MetS model using kidney-specific mosaic megalin knockout (KO) mice. Compared with control littermates fed a normal-fat diet, control littermates fed an HFD for 12 weeks showed autolysosomal dysfunction with autophagy impairment and increased expression of hypertrophy, lipid peroxidation, and senescence markers in PTECs of the S2 segment, peritubular capillary rarefaction with localized interstitial fibrosis, and glomerular hypertrophy with mesangial expansion. These were ameliorated in HFD-fed megalin KO mice, even though these mice had the same levels of obesity, dyslipidemia, and hyperglycemia as HFD-fed control mice. Intravital renal imaging of HFD-fed wild-type mice also demonstrated the accumulation of autofluorescent lipofuscin-like substances in PTECs of the S2 segment, accompanied by focal narrowing of tubular lumens and peritubular capillaries. In cultured PTECs, fatty acid–rich albumin induced the increased expression of genes encoding PDGF-B and monocyte chemoattractant protein-1 *via* megalin, with large (auto)lysosome formation, compared with fatty acid–depleted albumin. Collectively, the megalin-mediated endocytic handling of glomerular-filtered (lipo)toxic substances appears to be involved primarily in hypertrophic and senescent PTEC injury with autophagy impairment, causing peritubular capillary damage and retrograde glomerular alterations in HFD-induced kidney disease. Megalin could be a therapeutic target for obesity/MetS-related CKD, independently of weight, dyslipidemia, and hyperglycemia modification.

J Am Soc Nephrol 27: 1996–2008, 2016. doi: 10.1681/ASN.2015020190

Obesity is a serious health and economic problem worldwide.[1] Individuals with central obesity are predisposed to metabolic syndrome (MetS), which is characterized by the clustering of hyperglycemia, dyslipidemia, and hypertension, and are at high risk of cardiovascular disease-related mortality.[2] These individuals frequently have CKD, which is also an emerging risk factor for both cardiovascular disease and ESRD.[3]

Glomerular hypertrophy is a histologic feature reported originally in proteinuric patients with massive obesity.[4] In these patients, the pathogenesis

Received February 20, 2015. Accepted September 16, 2015.

S.K. and M.H. contributed equally to this work.

Published online ahead of print. Publication date available at www.jasn.org.

Present address: Dr. Akiyo Suzuki, Department of Cellular Neurobiology, Brain Research Institute, Niigata University, 1-757 Asahimachi-dori, Chuo-ku, Niigata 951-8585, Japan.

Correspondence: Dr. Akihiko Saito, Department of Applied Molecular Medicine, Niigata University Graduate School of Medical and Dental Sciences, 1-757 Asahimachi-dori, Chuo-ku, Niigata 951-8510, Japan. Email: akisaito@med.niigata-u.ac.jp

causing glomerular hypertrophy is likely to be associated with the development of glomerulosclerosis, which eventually worsens renal outcome.[5]

Megalin is a large (approximately 600 kDa) glycoprotein member of the low-density lipoprotein receptor family[6] that is expressed primarily at clathrin-coated pits and partly at the microvilli of proximal tubule epithelial cells (PTECs).[7] Megalin mediates intracellular signal transduction[8,9] and plays a pivotal role in the reabsorption of diverse glomerular-filtered substances, including albumin and low molecular weight proteins.[10] Kidney-specific megalin knockout (KO) mice established using the Cre/lox system,[11,12] as well as patients with Donnai–Barrow and facio-oculo-acoustico-renal syndromes caused by mutations in the megalin gene,[13] show albuminuria and low molecular weight proteinuria without apparent impairment of renal function. Albumin is an efficient carrier of fatty acids and advanced glycation end products, which mediate cellular lipotoxicity[14] and glycotoxicity,[15] respectively. Therefore, megalin is a candidate molecule for mediating renal lipo-glycotoxicity; however, its pathologic role in CKD remains to be determined.

In this study, we investigated the role of megalin in kidney alterations in a well-characterized high-fat diet (HFD)–induced obesity/MetS model[16] using kidney-specific megalin KO mice.[11]

RESULTS

Megalin KO and Control Mice Fed an HFD Show the Same Levels of MetS-Like Systemic Characteristics

In kidney-specific megalin KO (hereafter designated as megalin KO) mice (apoE *cre*, megalin *lox/lox*),[11] megalin gene deletion occurs in a mosaic pattern in approximately 60% of PTECs, thereby allowing a direct comparison between megalin KO and intact PTECs in the same mice. To enhance the manifestation of kidney disease and specify primarily pathogenic lesions, megalin KO and control littermate mice were left-uninephrectomized at 10 weeks of age and then subjected to feeding with an HFD or normal-fat diet (NFD) for 12 weeks. As shown in Table 1, two-way ANOVA of body weight, fasting blood glucose, and total cholesterol levels showed a significant association with diet (HFD versus NFD), but not with genotype (megalin KO versus control), and revealed no two-factor (diet-genotype) interaction. These results indicate that obesity/MetS-related systemic features[16] were manifested equally in megalin KO and control mice by feeding them an HFD. Kidney weight also showed a significant association only with diet and revealed no two-factor interaction.

Megalin Mediates Dysfunctional Autolysosome Accumulation in PTECs of the S2 Segment in HFD-Fed Mice, which Is Associated with Autophagy Impairment

The most prominent histologic feature in kidney sections of HFD-fed control mice was cytosolic vacuolar formation in PTECs that were immunostained with organic anion transporter 1 (OAT1), a marker for the S2 segment[17] (Figure 1A). Electron microscopy showed that the vacuoles contained OsO_4-stained multilamellar whirl structures (Figure 1B). The vacuolar membranes were immunostained with both lysosomal-associated membrane protein 1 (LAMP1), a lysosome marker, and microtubule-associated protein 1A/1B-light chain 3 (LC3), an autophagosome marker (Figure 1C), indicating that they were derived from dysfunctional autolysosomes particularly in the apical side of the cells.

Dysfunction of autolysosomes, the final sites of the autophagic pathway, is likely to be associated with impairment of this pathway in PTECs. To confirm this impairment, we used a transgenic mouse model that expresses green fluorescent protein (GFP)-LC3 systemically under the same experimental protocol as shown above (Supplemental Figure 1). p62, a marker of autophagy impairment, also accumulated in vacuolized PTECs and, to a lesser extent, in nonvacuolized PTECs of HFD-fed control mice (Figure 1D). These results indicate that HFD-induced autophagy impairment in PTECs is associated with autolysosomal dysfunction. HFD-induced autophagy impairment was reportedly caused by mammalian target of rapamycin complex 1 (mTORC1) activation.[18] However, we found that $S6^{Ser235/236}$ phosphorylation, a marker for mTORC1 activation, was increased by HFD feeding in only distal nephron segments and not in PTECs (Supplemental Figure 2).

In HFD-fed mosaic megalin KO mice, autolysosome-derived vacuoles were found exclusively in megalin-expressing PTECs, but scarcely in megalin KO PTECs, even in the OAT1-positive S2 segment (Figure 1E). A significant statistical interaction was

Table 1. Comparison of general and renal parameters in control and megalin KO mice fed an HFD or NFD

	KO-HFD	Cont-HFD	KO-NFD	Cont-NFD	*P* Values		
					Diet (HFD Versus NFD)	Genotype (KO Versus Cont)	Diet-Genotype Interaction
Body wt (g)	47.2±4.9	48.0±3.5	30.7±2.9	32.5±5.6	<0.001	0.17	0.94
KW (g)	0.28±0.03	0.26±0.03	0.25±0.04	0.23±0.03	0.002	0.18	0.44
BG (mmol/L)	6.11±1.45	5.83±1.32	3.33±0.65	3.88±0.81	<0.001	0.43	0.69
TC (mmol/L)	3.78±0.56	3.60±0.31	2.97±0.56	2.96±0.54	<0.001	0.72	0.79
FFA (μmol/L)	648.0±145.8	696.3±465.5	655.2±109.5	879.7±246.9	0.31	0.15	0.35
UAE (μg/day)	293.6±192.7	147.5±75.8	126.3±45.2	44.3±34.9	0.82	0.04	0.01

KW, kidney weight; BG, blood glucose; TC, total cholesterol; FFA, free fatty acids; Cont, control. *n*=10 in each group. Values are means±SD.

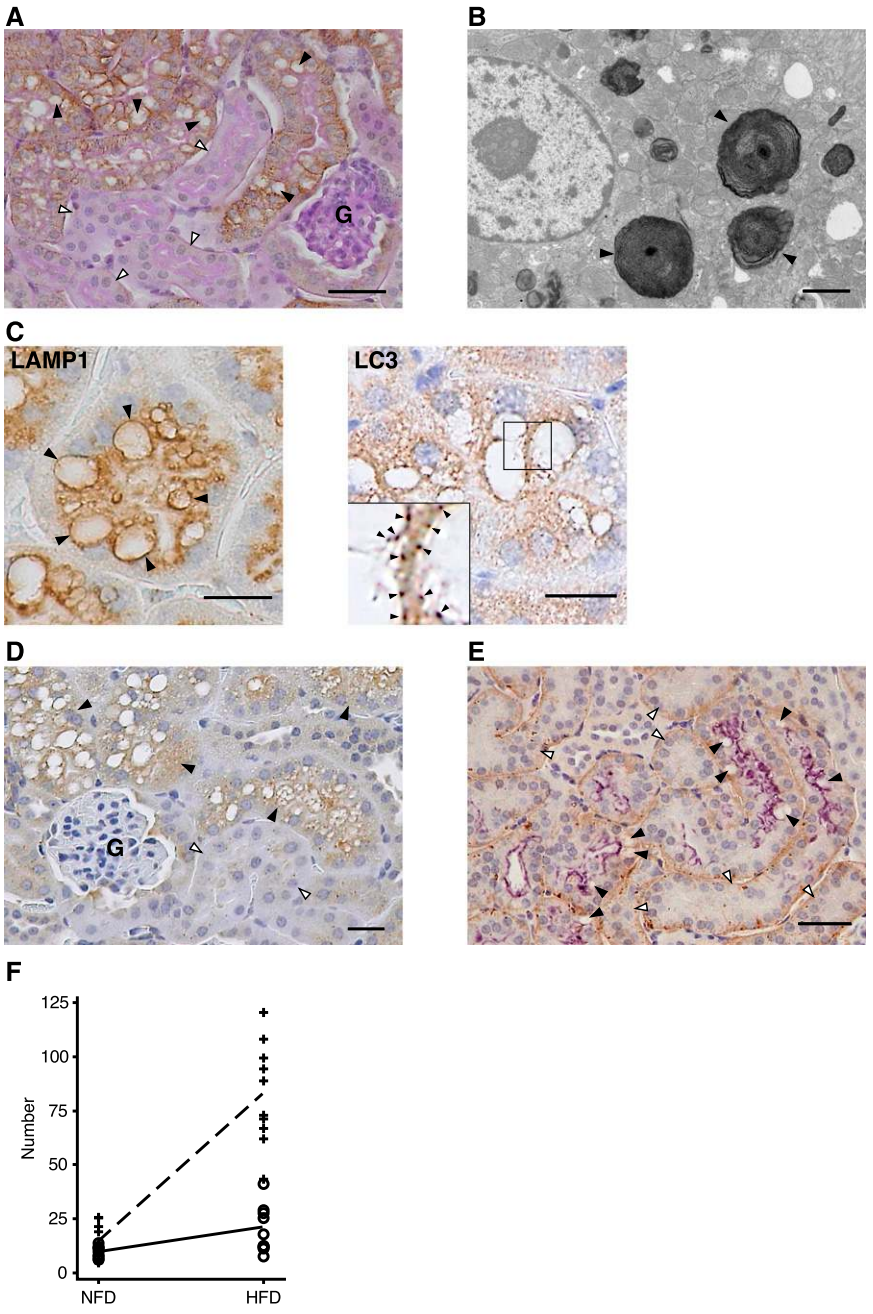

Figure 1. Megalin mediates dysfunctional autolysosome accumulation in PTECs of the S2 segment in HFD-fed mice, which is associated with autophagy impairment. (A) Giant vacuolizations were seen in OAT1-positive S2 segments of proximal tubules (closed arrowheads), but not in OAT1-negative ones (open arrowheads) in PAS-stained kidney sections of control mice fed an HFD for 12 weeks. Bar =50 μm. G, glomerulus. (B) Electron-dense multilamellar whirl structures (closed arrowheads) were detected in the cytoplasm of PTECs of HFD-fed control mice by electron microscopy. Bar =5 nm. (C) Immunostaining for LAMP1 and LC3 (closed arrowheads) in the vacuolar membranes of PTECs of HFD-fed control mice. Bar =20 μm. (D) p62 was heavily immunostained in vacuolized PTECs (closed arrowheads), but less so in nonvacuolized PTECs (open arrowheads) of HFD-fed control mice. Bar =20 μm. G, glomerulus. (E) In mosaic megalin KO mice fed an HFD, vacuolization was only seen in megalin (stained purple)-expressing PTECs (closed arrowheads), but not in megalin-KO PTECs in OAT1 (stained brown)-positive S2 segments (open arrowheads). Bar =20 μm. (F) Two-factor (diet-genotype) interaction plot by two-way ANOVA for mean number of vacuoles ($\geq$5 μm in diameter) counted per $\times$400 magnification field in five randomly selected cortical regions on PAS-stained kidney sections of mosaic megalin KO (○, solid line) and control mice (+, dashed line) fed an HFD or NFD (n=8 in each group). $P<0.001$.

found between diet and genotype in vacuolar formation by two-way ANOVA (Figure 1F), indicating that the HFD-induced vacuolization in PTECs was significantly inhibited in megalin KO mice compared with control mice. These results suggest that HFD-induced autolysosomal dysfunction and autophagy impairment in PTECs were caused primarily by megalin-mediated endocytosis, which is presumably involved in the uptake of toxic glomerular-filtered substances, affecting the function of the endosome/lysosome system of the S2 segment.

p27^{Kip1} Is Upregulated in PTECs of HFD-Fed Control Mice, but not in those of HFD-Fed Megalin KO Mice

In the present study, the nuclear expression of p27^{Kip1}, a marker of cell cycle inhibition and cellular hypertrophy, was more detectable in PTECs of HFD-fed control mice than in those of NFD-fed mice (Figure 2A). However, the number of nuclei immunostained for p27^{Kip1} in PTECs was significantly lower in HFD-fed megalin KO mice (Figure 2A), showing that p27^{Kip1} expression was increased in megalin-expressing PTECs with a hypertrophic phenotype, but not in megalin KO PTECs in the same kidney sections (Figure 2B). Hypertrophic tubules are likely to influence both intratubular and interstitial spaces, which should affect the structure and function of glomeruli in a retrograde manner.

Vacuolized PTECs in HFD-Fed Mice Show Evidence for Lipid Peroxidation and Cellular Senescence

The increased expression of p27^{Kip1} is also known as a marker of cellular senescence.[19] In intravital imaging in kidneys of HFD-fed wild-type mice using two-photon laser scanning microscopy, abnormal autofluorescence was found in PTECs (Figure 2C) that were located in the S2 segment (Supplemental Figure 3). The intracellular distribution and

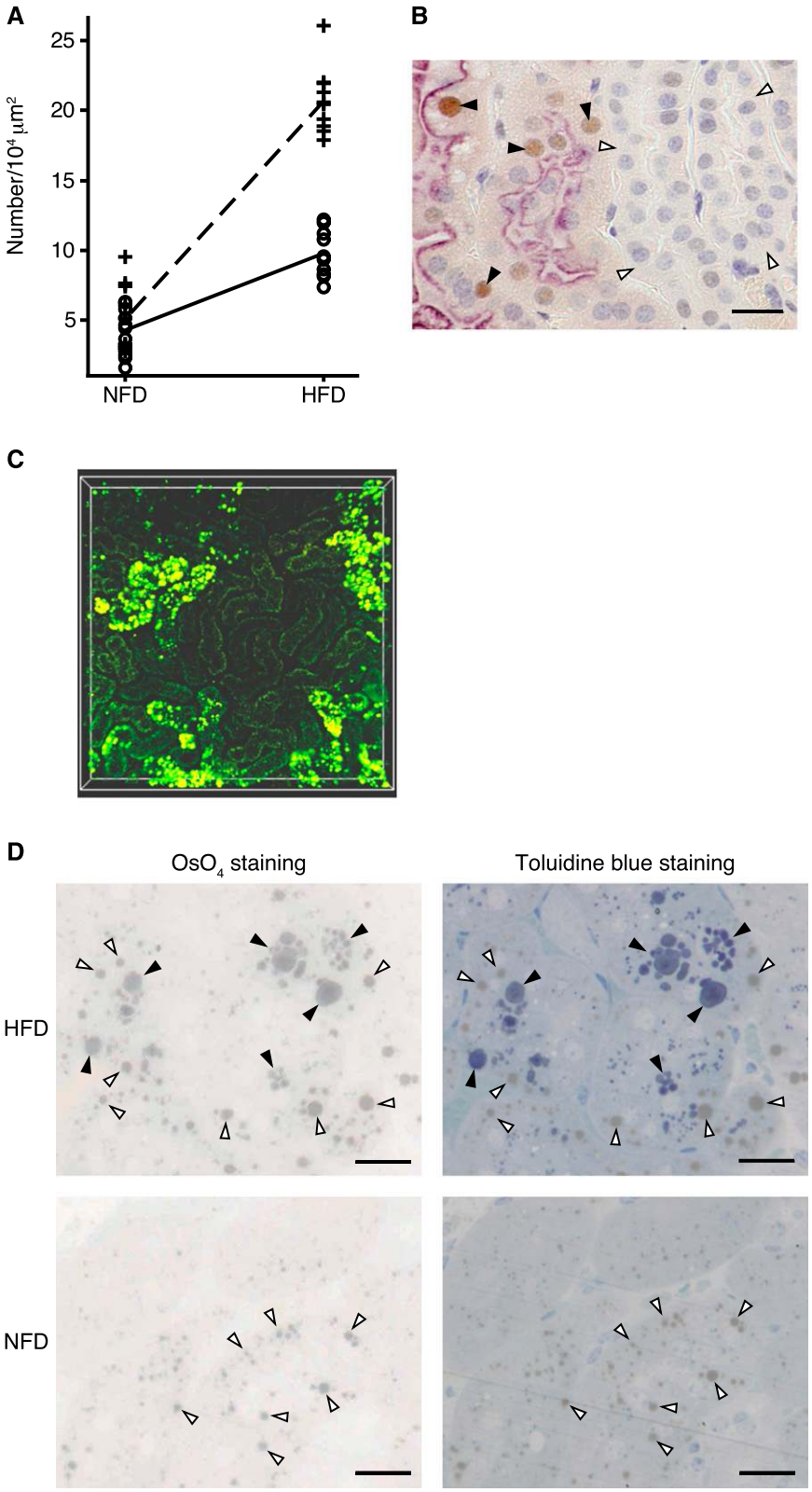

Figure 2. Megalin induces hypertrophic and senescent phenotypes in PTECs of mice fed an HFD. (A) Two-factor (diet-genotype) interaction plot for mean number of $p27^{Kip1}$-immunostained nuclei in five randomly selected PTEC regions (×800 magnification) on kidney sections of mosaic megalin KO (○, solid line) and control mice (+, dashed line) fed an HFD or NFD (n=10 in each group). The numbers are expressed per 10^4 μm^2 of PTEC area. $P<0.001$. (B) Double im-munostaining for $p27^{Kip1}$ (brown) and megalin (purple) demonstrated that megalin-expressing PTECs showed nuclear $p27^{Kip1}$ immunostaining (closed arrowheads) with hypertrophic changes that were barely seen in megalin-KO PTECs (open arrowheads) of megalin KO mice fed an HFD. Bar =20 μm. (C) Vacuolized PTECs showed strong autofluorescence (green-yellow) in intravital imaging in the kidneys of wild-type mice fed an HFD for 12 weeks. (D) In kidney sections fixed with glutaraldehyde and OsO_4, the contents of vacuoles (compatible to autolysosomes) were stained intensely with toluidine blue (closed arrowheads) in PTECs of HFD-fed control mice, whereas there were distinct, mostly smaller vesicles in the basal side, which were stained with OsO_4 but not with toluidine blue and also seen in some PTECs of NFD-fed control mice (open arrowheads, putative "lipid droplets"). Bar =20 μm.

tubular localization patterns of the autofluorescent substances indicated that they were contained in dysfunctional autolysosomes of PTECs. Such autofluorescence was not detected in the vacuoles of PTECs in frozen kidney sections of HFD-fed LC3-GFP transgenic mice (Supplemental Figure 1, A and B), probably because the lysosomal contents were leaky from weakly fixed tissue sections.[20] As shown previously,[21] the contents of dysfunctional autolysosomes were stained with Luxol Fast Blue, but not with Oil Red O, indicating that they contain phospholipids and not neutral triglycerides (Supplemental Figure 4, A and B). Furthermore, the vacuolar contents were stained intensely with toluidine blue in kidney tissues fixed with glutaraldehyde and OsO_4 (Figure 2D), indicating that they have a lipofuscin-like senescent character.[22,23] The vacuolar contents, as well as the cytoplasm around the vacuoles, were also immunostained for 4-hydroxy-2-nonenal (4HNE) (Supplemental Figure 4C), a marker for lipid peroxidation of unsaturated fatty acids[24] and a potential source of fluorescent chromophores.[25] In HFD-fed control mice, unsaturated fatty acids used for lipid peroxidation in the vacuoles or cytoplasm may be derived from increased glomerular-filtered, fatty acid–bound albumin or other megalin-mediated carrier proteins, including

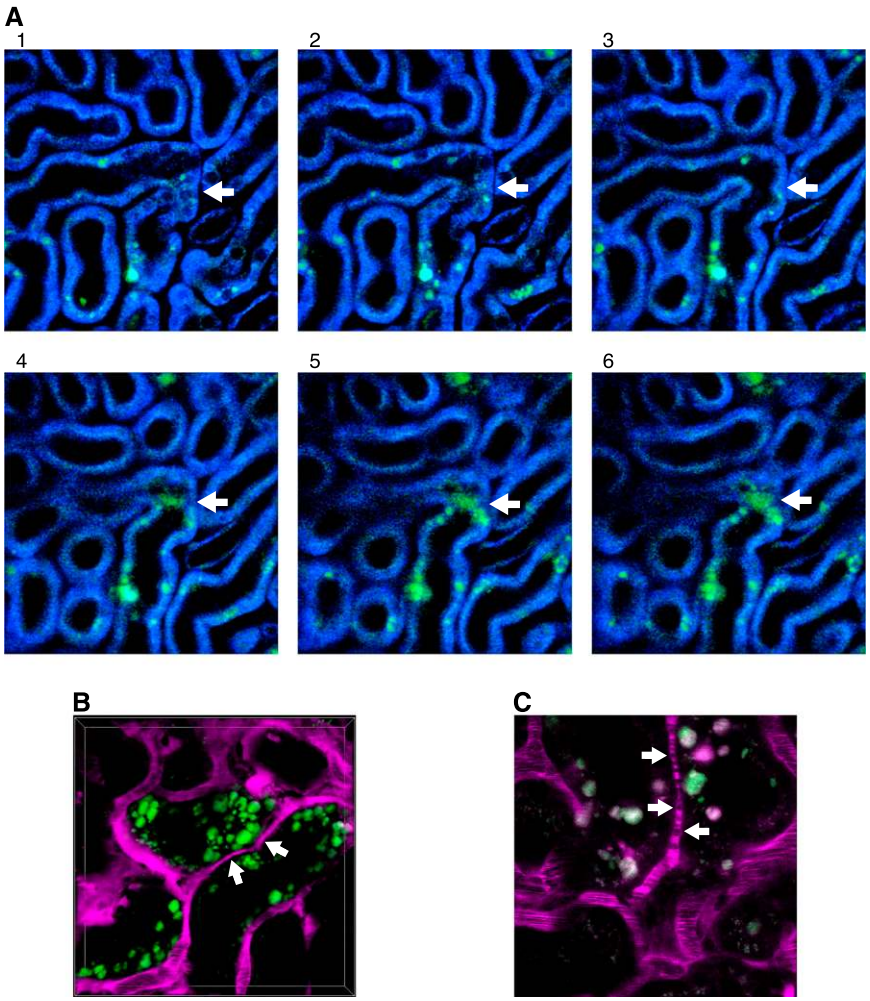

Figure 3. Intravital imaging reveals narrowing of proximal tubular lumens and peritubular capillaries in the kidney of HFD-fed C57BL/6J mice. (A) Z-stack images showed narrowing of the tubular lumen in the regions where autofluorescent vacuoles accumulated in PTECs. The arrows indicate the same part of the tubule in six different z planes (A1 [superficial] to A6 [16 μm deeper than A1]). (B) The peritubular capillary indicated by the arrows between two vacuolized tubules showed a smaller diameter than the other capillaries (magenta: Rhodamine B-conjugated 70-kDa dextran). (C) The peritubular capillary indicated by the arrows showed disturbed blood cell flow with leukocyte attachment that was visualized by clear, rounded shadows.

apolipoproteins,[26] even though free fatty acid concentrations in the serum were not significantly different between NFD- and HFD-fed mice (Table 1).

Intravital Imaging in the Kidney of HFD-Fed Mice Shows Narrowing of Tubular Lumens and Peritubular Capillaries Adjacent to PTECs Containing Autofluorescent Lipofuscin-Like Substances in the S2 Segment

In intravital imaging in kidneys of HFD-fed mice, excitation by a 720-nm laser, which can reveal cell shapes by visualization of cytosolic and mitochondrial NADH,[27,28] showed that the tubular lumens were narrowed at the regions where autofluorescent lipofuscin-like substances accumulated in the PTECs (Figure 3A). Rhodamine B-conjugated 70-kDa dextran was then administered intravenously to visualize plasma. As blood cells are not excited by the laser, they are seen as shadows in the magenta plasma flow. Peritubular capillaries between vacuolized PTECs were narrowed (Figure 3B) and blood cell flow was disturbed (Figure 3C), features that were observed rarely in NFD-fed mice.

Peritubular Capillary Rarefaction Is Evident in HFD-Fed Control Mice, but not in HFD-Fed Megalin KO Mice

Peritubular capillary narrowing or obstruction was also found by electron microscopy in HFD-fed control mice, but scarcely in NFD-fed control mice (Figure 4A). This finding was accompanied by localized interstitial fibrosis (Figure 4, A and B), which was likely to be induced by activated fibroblasts/pericytes.[29] Hence, we evaluated damage in peritubular capillaries *via* immunohistochemistry for CD31, an endothelial marker, in both HFD- and NFD-fed mice. Peritubular capillary rarefaction was more pronounced in HFD-fed control mice than in those fed an NFD (Figure 4C). In contrast, rarefaction was not evident in HFD-fed megalin KO mice (Figure 4, C and D). These results indicate that the HFD-induced, megalin-mediated phenotype changes in PTECs are likely to be involved in peritubular capillary damage.

Glomerular Hypertrophy and Mesangial Matrix Expansion Are Observed in HFD-Fed Control Mice, but Are Ameliorated in HFD-Fed Megalin KO Mice

By univariate (correlation matrix) and multivariate (principal component analysis) statistical analyses, urinary albumin excretion (UAE) was found to be associated with kidney weight rather than body weight. Hence, kidney weight appeared to be a confounding factor of UAE for the diet-genotype factors. Thus, we carried out two-way analysis of covariance, adjusted using kidney weight as a covariate, for UAE as a dependent variable and the diet-genotype factors as fixed effects, showing a significant diet-genotype interaction for UAE (Table 1). Namely, although UAE levels were higher in megalin KO mice, even in those fed an NFD, as megalin mediates albumin uptake in PTECs, UAE was less enhanced by diet (HFD) in megalin KO mice than in control mice. Histologic analysis also showed that HFD-induced glomerular hypertrophy with

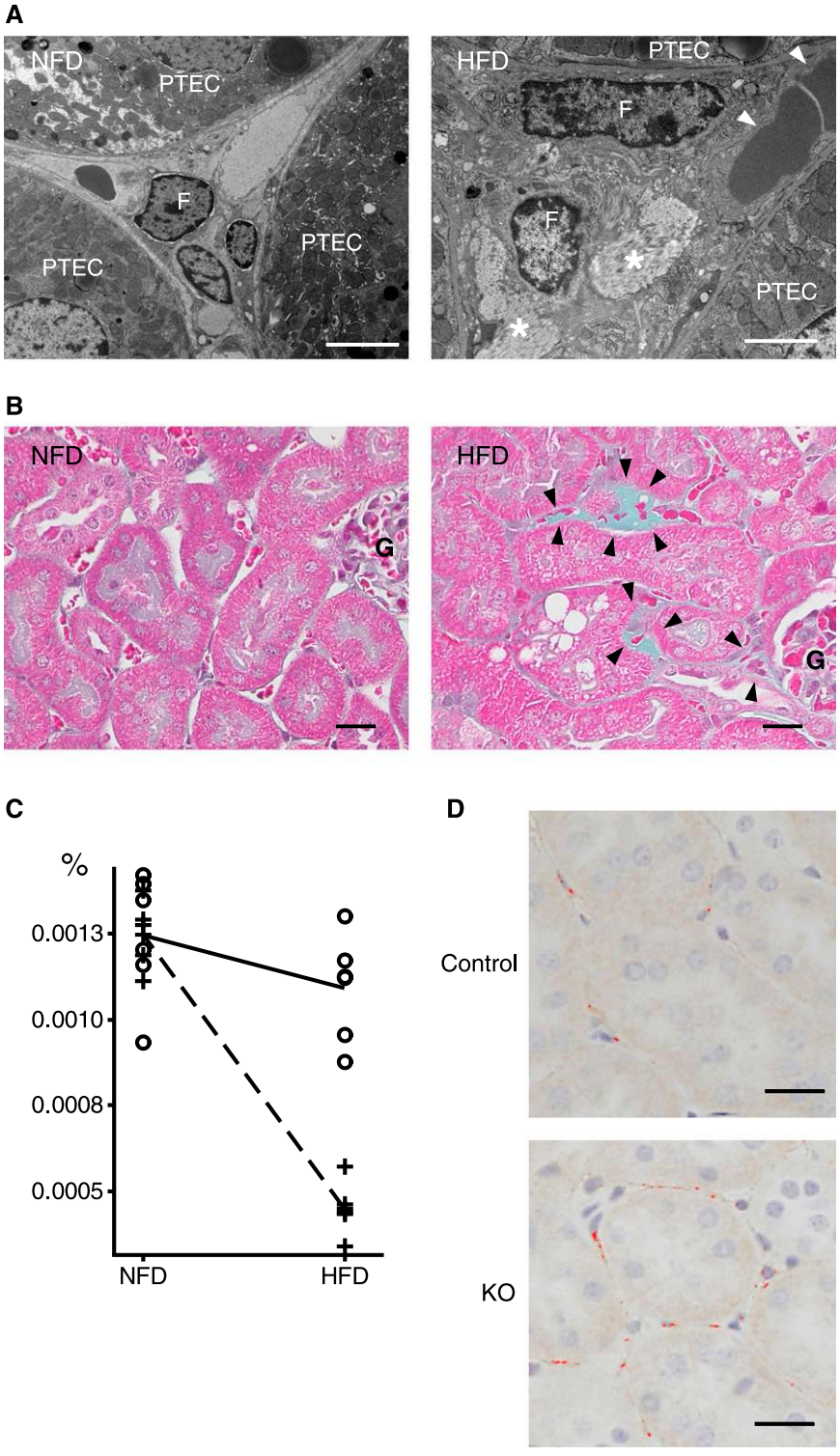

Figure 4. Damage to peritubular capillaries is seen in control mice fed an HFD, but is attenuated in HFD-fed megalin KO mice. (A) Localized interstitial fibrosis (asterisks) and peritubular capillary obstruction (arrowheads) were demonstrated by electron microscopy in control mice fed an HFD, but not in those fed an NFD. F, fibroblast/pericyte. Bar =5 nm. (B) Masson trichrome staining of the kidney sections also showed localized interstitial fibrosis (arrowheads) in control mice fed an HFD, but not in those fed an NFD. Bar =20 μm. G, glomerulus. (C) Two-factor (diet-genotype) interaction plot for mean CD31-immunostained endothelial areas (%) in ten randomly selected cortical regions (×400 magnification) of mosaic megalin KO (○, solid line) and control mice (+, dashed line) fed an HFD or NFD (n=6 in each group). $P<0.001$. (D) Representative photomicrograph showing CD31 immunostaining on peritubular capillaries, colored red using Image-Pro Plus v.7.0, in control and KO mice fed an HFD. Bar =20 μm.

mesangial matrix expansion was less evident in both the superficial and juxtamedullary cortical regions in megalin KO mice compared with control mice (Figure 5). Collectively, HFD-induced tubuloglomerular alterations are likely to be caused by a megalin-mediated mechanism.

Giant (Auto)lysosomes Accumulate More in Cultured PTECs following Incubation with Fatty Acid–Rich Albumin than with Fatty Acid–Depleted Albumin

Hyperglycemic factor(s) *per se* may not be apparently involved in megalin-mediated autolysosomal vacuolization in PTECs, because there is scarcely such a finding in a streptozotocin-induced type 1 diabetes model (data not shown). To examine the megalin-mediated mechanism associated with dyslipidemia, we performed *in vitro* experiments using megalin-expressing immortalized rat proximal tubule cells (IRPTCs) or IRPTCs stably expressing enhanced green fluorescent protein (EGFP)-LC3, an autophagosome marker. The cells were incubated with albumin, an endocytic ligand of megalin that had been either enriched in or depleted of fatty acids as a lipotoxic model. Compared with fatty acid–depleted albumin, incubation of IRPTCs with fatty acid–rich albumin induced an increase in intracellular giant vacuolar formation, as detected using the lysosomal marker LysoTracker (Figure 6A). These giant vacuoles were sometimes surrounded by an EGFP-LC3 signal (Figure 6B) in IRPTCs expressing EGFP-LC3, indicating that they were derived from lysosomes or autolysosomes. These results suggest that the cellular uptake of lipotoxic proteins may be involved in giant (auto)lysosome formation in PTECs. Autophagy flux in IRPTCs was also inhibited by using fatty acid–rich

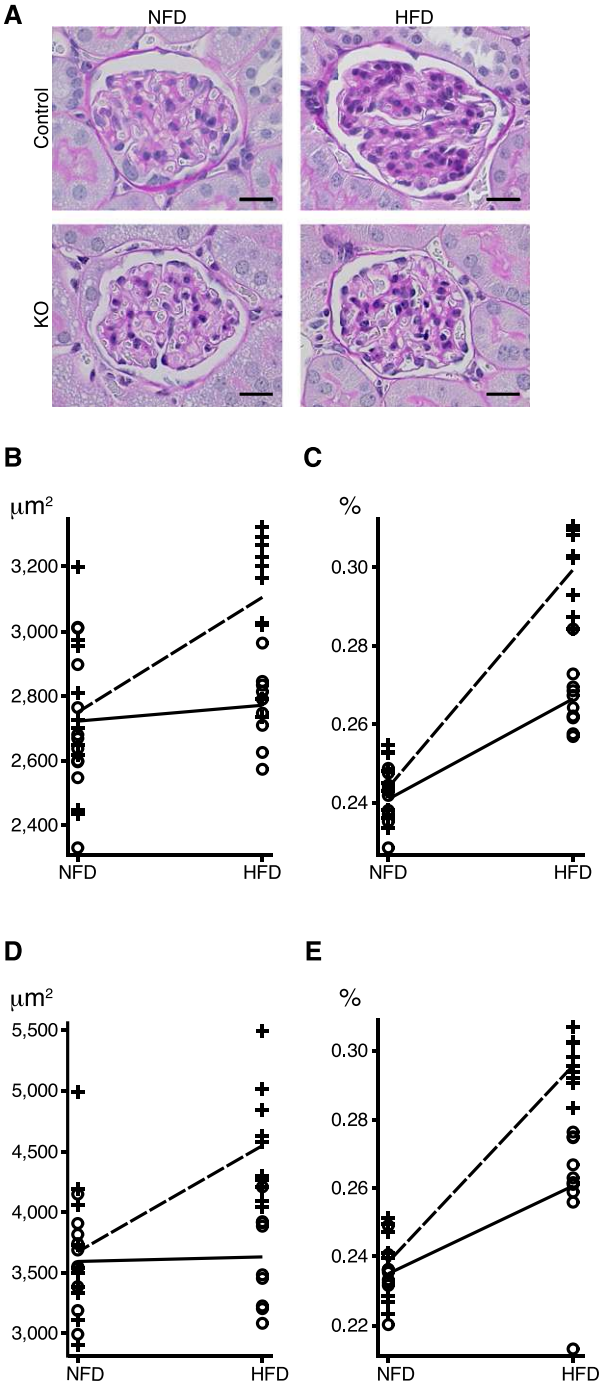

Figure 5. Glomerular hypertrophy with mesangial matrix expansion seen in HFD-fed control mice is ameliorated in megalin KO mice fed an HFD. (A) Representative photomicrographs illustrating PAS-stained glomeruli in the juxtamedullary cortical regions of megalin KO and control mice fed an HFD or NFD. Bar =10 μm. Two-factor (diet-genotype) interaction plots are shown for mean (B and D) glomerular and (C and E) mesangial matrix areas (percentage of the glomerular areas) in 15 randomly selected glomeruli (×800 magnification) in both the (B and C) superficial and (D and E) juxtamedullary cortical regions of megalin KO (○, solid line) and control mice (+, dashed line) fed an HFD or NFD (n=10 in each group). (B) $P<0.05$; (C, D, and E) $P<0.01$.

albumin compared with fatty acid–depleted albumin (Supplemental Figure 5).

Megalin Mediates the Upregulation of PDGF-B and Monocyte Chemoattractant Protein-1 Expression in Cultured PTECs Incubated with Fatty Acid–Rich Albumin

The transition of interstitial fibroblasts/pericytes to myofibroblasts is activated *via* signaling mediated by α and β receptors for PDGF (PDGFRα and PDGFRβ).[30,31] A major ligand of both PDGFRα and PDGFRβ,[32] PDGF-B, is known to induce tubulointerstitial fibrosis,[33] and the tubular expression of PDGF-B is upregulated in a unilateral ureteral obstruction model.[30] We found that PDGF-B was upregulated in IRPTCs incubated with fatty acid–rich albumin rather than with fatty acid–depleted albumin (Figure 6C). Knockdown of megalin expression in the cells using specific small interfering RNA (siRNA) (approximately 46% suppression of megalin protein expression, Supplemental Figure 6) suppressed the fatty acid–rich albumin mediated upregulation of PDGF-B (approximately 44% suppression of the mRNA expression, Figure 6C). These results indicated that the megalin-mediated handling of lipotoxic proteins may be involved directly in the increased expression of PDGF-B in PTECs. Similar data were also obtained for monocyte chemoattractant protein-1 (MCP-1), a chemokine involved in inflammation (Figure 6C).

Collectively, the pathways of the megalin-mediated mechanism of tubuloglomerular alterations in HFD-induced kidney disease are illustrated in Figure 7.

DISCUSSION

Using kidney-specific megalin KO mice crossbred with an experimental nephrotic model of inducible podocyte injury for nonselective glomerular protein filtration, megalin was found to initiate PTEC damage by reabsorbing massive proteins into the cells.[34] However, there is a conflicting report using a glomerular injury model with antiglomerular basement membrane serum in the KO mice, which indicated that megalin-mediated endocytosis may not be associated primarily with the development of tubulointerstitial damage.[35] Because both analyses were performed using acute nephrotic models with overwhelming glomerular damage, further studies are required to clarify the role of megalin in slowly progressing CKD models.

In the current study, using an HFD-induced kidney disease model with low-grade proteinuria, we determined that autolysosomal dysfunction was induced by the megalin-mediated endocytic handling of qualitatively toxic substances in PTECs. We found that lipotoxicity by fatty acid–bound albumin is a candidate for megalin-mediated pathogenesis. However, apolipoproteins[26] and/or obesity/MetS-associated molecules, such as adipokines released from visceral adipocytes, may also be involved in the megalin-mediated mechanism. Further studies are needed to elucidate how these toxic substances trigger intracellular pathogenic pathways *via* megalin.

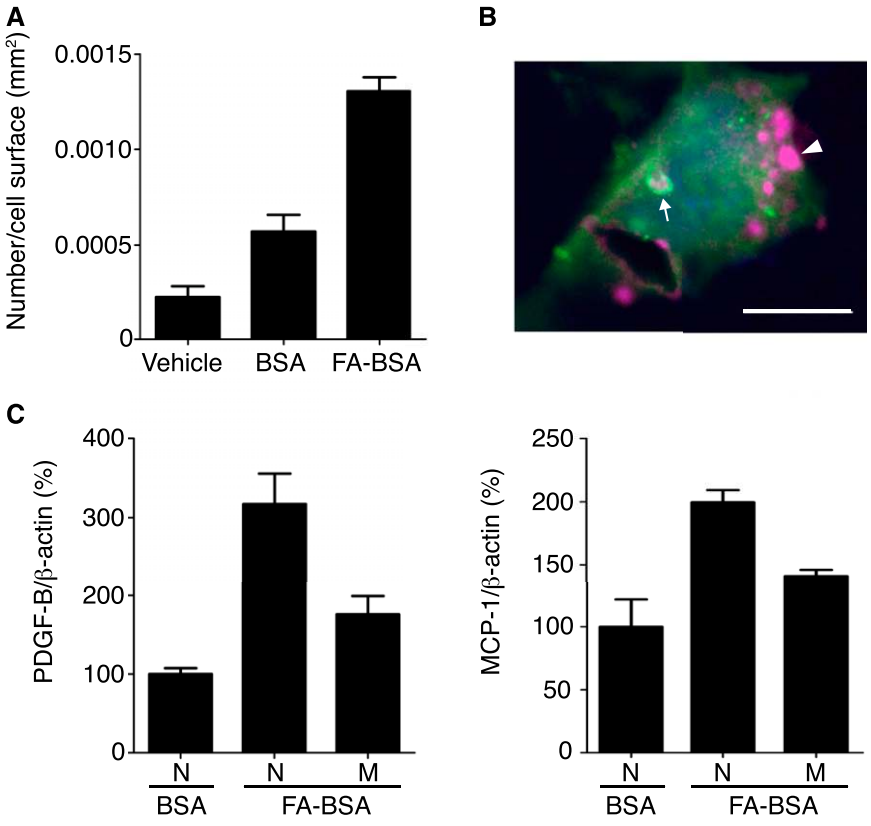

Figure 6. Fatty acid–rich albumin induces giant (auto)lysosome formation and increases PDGF-B and MCP-1 mRNA expression *via* megalin in cultured IRPTCs. (A) After incubation with 1 mg/ml fatty acid–depleted BSA (BSA), fatty acid–rich BSA (FA-BSA), or vehicle (PBS) for 24 hours, the number of giant lysosomes (LysoTracker-positive areas >3.0 μm^2) was counted in 20 randomly selected IRPTCs. Values are means±SEM in triplicate experiments. (B) IRPTCs stably expressing EGFP-LC3 incubated with 1 mg/ml FA-BSA for 24 hours showed large lysosomes (LysoTracker-positive, arrowhead) or autolysosomes (EGFP-LC3-encircled, LysoTracker-positive; arrow) (LysoTracker-positive areas >3.0 μm^2). EGFP-LC3, green; LysoTracker, magenta; and 4′,6-diamidino-2-phenylindole , blue. Bar =10 μm. (C) PDGF-B and MCP-1 mRNA levels in IRPTCs transfected with megalin siRNA (M) or negative control siRNA (N) were analyzed by real-time RT-PCR, showing approximately 44% and 30% suppression of FA-BSA–mediated expression, respectively, by megalin knockdown. The relative percentages are shown by the average ratio with the cells transfected with negative control siRNA and treated with BSA. Values are means±SEM of the relative percentages in triplicate experiments.

Additionally, we found that HFD-induced, megalin-mediated autolysosomal dysfunction in PTECs is also associated with autophagy impairment. Autophagy protects PTECs in ischemia-perfusion,[36,37] drug toxicity,[38] and protein-overload nephropathy models.[18] Autophagy impairment is also likely to affect PTEC functions in HFD-induced kidney disease. Megalin-mediated autolysosomal dysfunction may also be associated with the generation of profibrotic and/or inflammatory signals in PTECs *via* the NLRP3 (NACHT, LRR, and PYD domain-containing protein 3) inflammasome pathway.[39]

The reason why PTECs in the S2 segment are susceptible to HFD-induced autolysosomal injury also remains unknown. The S1 segment is the major site for physiologic protein reabsorption.[40] However, under proteinuric conditions, pathologic ligands of megalin may overflow to the S2 segment where megalin is expressed more prominently in microvilli than in the S1 and S3 segments.[7] Subsequently, lysosomal enzyme function in the S2 segment may be impaired by toxic protein degradation load, resulting in the accumulation of lipofuscin-like substances *via* lipid peroxidation of unsaturated fatty acids, which is similar to the findings in aging kidneys.[41]

On the basis of our data, megalin could be a novel pharmacologic target for preventing or treating obesity/MetS-related CKD, such as by competing with megalin binding to toxic ligands or by suppressing megalin expression to reduce the uptake of these ligands into PTECs. Bardoxolone methyl, an Nrf2 activator, may be such a candidate drug, because it reportedly suppresses renal megalin expression in monkeys[42] and improves eGFR in CKD patients with type 2 diabetes.[43] However, megalin-mediated endocytosis in PTECs plays an important physiologic role in some processes such as vitamin homeostasis.[10] Therefore, complete megalin suppression may not be desirable. However, the megalin KO mice used in this study were deficient for megalin expression in approximately 60% of PTECs, but histologic tubuloglomerular alterations were significantly ameliorated. Thus, obesity/MetS-related CKD could be prevented effectively or treated by just partial pharmacologic megalin blocking, with vitamin supplementation if necessary.

In conclusion, the megalin-mediated endocytic handling of glomerular-filtered (lipo) toxic substances is involved primarily in hypertrophic and senescent PTEC injury with autophagy impairment, causing peritubular capillary damage and retrograde glomerular alterations in HFD-induced kidney disease. Blocking or suppressing the function of megalin would be a novel prophylactic or therapeutic strategy for obesity/MetS-related CKD, independently of the modification of weight and metabolic parameters such as dyslipidemia and hyperglycemia.

CONCISE METHODS

Induction of HFD-Induced Kidney Disease in Mice

Male kidney-specific megalin KO mice (apoE *cre*, megalin *lox/lox*) established by Professor Thomas Willnow (Max Delbrück Center

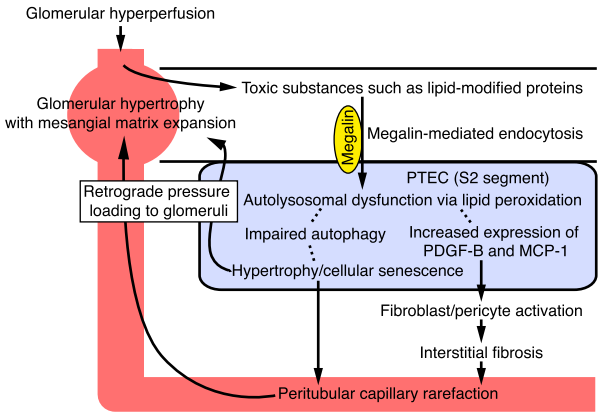

Figure 7. The megalin-mediated mechanism appears to be involved primarily in HFD-induced tubuloglomerular injury. In the presence of glomerular hyperperfusion that should occur in HFD-fed hyperglycemic mice, the megalin-mediated uptake of glomerular-filtered (lipo)toxic substances into PTECs may cause autolysosomal dysfunction *via* lipid peroxidation associated with autophagy impairment, leading to hypertrophic and senescent changes of PTECs. In addition, these processes may be associated with the increased production of profibrotic and inflammatory mediators, such as PDGF-B and MCP-1, which activate interstitial fibrocytes/pericytes to induce localized interstitial fibrosis. Peritubular capillaries would thereby become damaged and rarefactional by these complex mechanisms. These factors for glomerular hyperperfusion and increased tubular and peritubular capillary resistance should contribute to the development of glomerular hypertrophy with mesangial matrix expansion.

for Molecular Medicine, Germany)[11] and maintained on the C57BL/6J background,[34] as well as their littermate male control mice (megalin *lox/lox*), were used for this study. As fewer nephrons are found in patients with obesity/MetS-related kidney disease,[44] to promote the development of obesity/MetS-related kidney disease, the mice were left-uninephrectomized at 10 weeks of age before being fed *ad libitum* an HFD (60% of total calories from fat) or NFD (10% of total calories from fat) obtained from Research Diets (New Brunswick, Canada) from 11 weeks of age for 12 weeks. Urine was collected for 24 hours in metabolic balance cages, after which the mice underwent body weight measurement and blood sampling and were euthanized by saline perfusion *via* the left ventricle under intraperitoneal (ip) pentobarbital sodium anesthesia (50 mg/kg). Right kidneys were removed, weighed, and used for morphologic examinations and immunohistochemistry. GFP-LC3 #53 transgenic mice purchased from the RIKEN BioResource Center (Tsukuba, Japan) were also treated with the same experimental protocol and kidney sections were used for fluorescence microscopy observations. All animal experiments in this study were based on the National Institutes of Health Guide for the Care and Use of Laboratory Animals and approved by the institutional animal care and use committees of Niigata and Kagawa Universities.

Blood and Urine Analyses

Blood glucose concentrations were measured by using FreeStyle Freedom (Nipro). Total cholesterol and free fatty acids were assayed by enzymatic methods. Urinary albumin was measured by a quantitative turbidimetric immunoassay method (Wako Pure Chemicals).

Preparation of Kidney Sections for Light Microscopy

From horizontal cross-sections containing the hila of kidneys, 3-mm thick tissues were obtained and fixed in a 4% paraformaldehyde phosphate buffer for 72 hours at room temperature. After fixation, the tissues were dehydrated in a graded ethanol series from 70% to 100%, cleared in xylene, and embedded in paraffin. From each tissue sample, 2-μm thick sections were cut using a microtome (REM-710; Yamato Kohki Industrial Co., Ltd.) and used for staining with periodic acid–Schiff (PAS) or Masson trichrome. In addition, 4-μm thick sections were used for Luxol Fast Blue staining. Kidney tissue samples were snap-frozen in liquid nitrogen and prepared for Oil Red O staining. Additionally, the HFD-fed mice were perfused transcardially with a 0.9% saline and 4% paraformaldehyde phosphate buffer under ip anesthesia with pentobarbital sodium (50 mg/kg) and kidney sections were fixed in a 4% paraformaldehyde phosphate buffer overnight and embedded in OCT compound (Sakura Finetek). Subsequently, 4-μm thick frozen sections were cut with a cryostat (CM1850; Leica) for immunohistochemical analysis of 4HNE.

Immunohistochemistry

Kidney tissue sections were deparaffinized by immersion in xylene and rehydrated through a graded ethanol series. Antigen retrieval was accomplished by heating the slides in a microwave in 10 mM citrate buffer, pH 6.0. To eliminate endogenous peroxidase activity, the sections were incubated in 3% H_2O_2. Following incubation with 5% goat serum to block nonspecific binding, the sections were incubated for 30 minutes at room temperature with a primary antibody against OAT1 (1:40; KE038; Trans Genic, Inc.), LAMP1 (1:200; ab24170; Abcam, Inc.), LC3 (1:1,000; PM036; MBL), or p62/SQSTM1 (1:3,000; PM045; MBL), and overnight with phospho-S6 ribosomal protein XP rabbit monoclonal antibody (1:400; 4858; Cell Signaling Technology). This step was followed by sequential incubation with biotinylated goat anti-rabbit IgG (1:200; Vector Laboratories) and avidin-biotin-peroxidase complex (Elite ABC kit; Vector Laboratories). Finally, peroxidase activity was visualized with the 3,3′-Diaminobenzidine substrate-chromogen system (Dako), counterstained with Mayer hematoxylin or PAS, and examined under a light microscope. Frozen sections were also stained with an anti-4HNE antibody (1:200; ab46545; Abcam, Inc.) and the avidin-biotin-peroxidase complex method described above. Negative control staining was always performed in parallel by incubating sections with PBS instead of the primary antibodies.

For immunohistochemical staining with an anti-CD31 antibody, antigen retrieval was performed using proteinase K. Endogenous biotin activity was blocked with an avidin/biotin blocking kit (Vector Laboratories) prior to incubation with a rat anti-mouse CD31 antibody (1:100; ab56299; Abcam) at 4°C overnight. A biotinylated mouse-absorbed, rabbit anti-rat IgG antibody (1:500; Vector Laboratories) was used as a secondary antibody. Double immunostaining was also performed with paraffin sections of mouse kidney specimens. The sections were incubated sequentially with either an anti-OAT1 or anti-$p27^{Kip1}$ (phospho S10) antibody (1:50; ab62364; Abcam, Inc.) and horseradish peroxidase-labeled polymer anti-rabbit antibody (EnVision+ System; Dako).

Immunoreactivity was developed with the 3,3′-Diaminobenzidine substrate-chromogen system (Dako). Then, the sections were incubated with an anti-megalin antibody (1:3,000)[45] and detected with the avidin-biotin-peroxidase complex method described above, except that a VIP substrate kit (Vector Laboratories) was used. Counterstaining was performed with Mayer hematoxylin.

Electron Microscopy

For electron microscopy examination, the tissues (1-mm cubes) were fixed in a 2.5% glutaraldehyde solution in 0.1 M phosphate buffer, pH 7.4, and then in a 2.0% OsO_4 solution in the same buffer. They were dehydrated with an ethanol series and embedded in Poly/Bed812 (Polysciences, Inc.). Ultrathin sections (75–80 nm) were obtained on a Porter-Blum MT-1 ultramicrotome (Sorvall, Inc.), placed on 100-mesh grids, and stained with a tannic acid and lead solution.

Staining of Renal Sections with Toluidine Blue

After fixing kidney tissues with glutaraldehyde and OsO_4 and embedding them in Poly/Bed812, as described above, semithin sections mounted on glass slides were stained with a 1% toluidine blue dye solution including sodium borate on a slide warmer at 80°C for 5 seconds.

Preparation of Kidney Tissues from LC3-GFP Transgenic Mice

After the left kidneys were removed at 10 weeks of age, male GFP-LC3 #53 transgenic mice were fed an HFD or NFD for 12 weeks. Five mice fed an HFD or NFD were starved for 24 hours before euthanization and another five mice fed an HFD or NFD were euthanized under *ad libitum* conditions. Under ip pentobarbital sodium anesthesia (50 mg/kg), the mice were perfused transcardially with a 0.9% saline and 4% paraformaldehyde solution. The right kidneys were removed, dissected, and fixed in a 4% paraformaldehyde solution overnight at 4°C. Then, the samples were immersed in 15% sucrose/PBS for 4 hours and 30% sucrose/PBS for 4 hours, embedded in OCT compound, and stored at –70°C. For examination with a fluorescence microscope, 5-μm thick sections were prepared using a cryostat (CM1850; Leica) and mounted on glass slides. Well dried sections were washed with PBS for 5 minutes and stained with 4′,6-diamidino-2-phenylindole (dilution: 1:10,000; KPL) in the dark for 5 minutes. After washing with PBS for 10 seconds, the sections were mounted with SlowFade Gold Antifade Reagent (Life Technologies).

Evaluation of Autophagosomes in PTECs of LC3-GFP Transgenic Mice

Cryosections were examined using a fluorescence microscope (BZ-9000; Keyence) with a ×60 oil-immersion objective lens. Images captured for GFP-LC3 signals (autophagosomes) were detected specifically in PTECs by using a GFP filter, and not by using a tetramethylrhodamine isothiocyanate filter, in five randomly selected cortical regions of each sample (n=5 in each group). The images were analyzed using image processing and measuring software (Image-Pro Plus v.7.0; Media Cybernetics) to count the number of GFP-LC3 dot signals and measure the area of the proximal tubules. The results were expressed as the mean number of signals per 100 μm^2 area of the proximal tubules and the mean values of each mouse were evaluated statistically. All morphometric analyses in this study were performed by an investigator masked to sample identity.

Counting the Number of Dysfunctional Autolysosome-Derived Intracellular Vacuoles in PTECs and $p27^{Kip1}$ Immunostained Nuclei

Images of five cortical regions (×400 magnification) containing no glomeruli were taken randomly from PAS-stained kidney sections of megalin KO and control mice fed an HFD or NFD (n=8 in each group) using a BZ-8000 microscope (Keyence). The images were used to count the number of intracellular vacuoles (dysfunctional autolysosomes) with a diameter of 5 μm or more per field using Image-Pro Plus v.7.0. Similarly, images of five cortical regions (×800 magnification) were taken randomly from $p27^{Kip1}$-immunostained kidney sections of these mice (n=10 in each group) using a BZ-8000 microscope to count the number of positively $p27^{Kip1}$-immunostained nuclei, expressed as per 10^4 μm^2 of PTEC area. The mean values of each mouse were evaluated statistically.

In Vivo Multiphoton Imaging

In vivo imaging was performed as reported previously[46] using an Olympus FV1000MPE multiphoton imaging system powered by a Chameleon Ultra-II MP laser at 720 nm and 860 nm (Coherent, Inc.). Male C57BL/6J mice (Japan SLC, Inc.) were right-nephrectomized at 7 weeks of age and fed an HFD for 12 weeks. The mice were then anesthetized with isoflurane (2%) and tracheotomized. The jugular vein was cannulated for fluorescent dye injection and the left kidney was exteriorized through a small flank incision. Both microscope stage and animals were warmed using a heating pad during all experimental procedures. The microscope objective was a ×25 water-immersion lens with a 1.05 numerical aperture. After obtaining images from mice with excitations at 720 nm and 860 nm without exogenous fluorescent dye, a bolus of Lucifer yellow (molecular mass 457 Da) (100 μg/kg; Invitrogen), which is filtered freely by glomeruli, was injected intravenously to localize the proximal tubular segments. In addition, rhodamine B-conjugated 70-kDa dextran (3 mg/kg; Invitrogen) was injected intravenously to visualize plasma. Three-dimensional images were taken at a depth of 5 μm to 25–35 μm (1 μm apart) from the surface of the kidney using equivalent detector sensitivities and laser powers. The images were reconstructed as a z-stack image (20–30 μm thick). Time-lapse imaging at 512×512 resolution was obtained by 20 consecutive images with 2-second intervals for each picture.

Evaluation of Peritubular Capillary Rarefaction

After immunostaining of CD31, images of ten cortical regions (×400 magnification) containing no glomeruli were selected randomly from megalin KO and control mice fed an HFD or NFD (n=6 in each group) using a BZ-8000 microscope and used to evaluate CD31-positive areas in the renal cortex with Image-Pro Plus v.7.0. The CD31-positive areas were expressed as percentages of the field and the mean values of each mouse were evaluated statistically.

Evaluation of Glomerular Sizes and Mesangial Matrix Areas

For morphometric analysis, the superficial and juxtamedullary cortical regions were chosen randomly (×200 magnification) in megalin KO and control mice fed an HFD or NFD (n=10 in each group) and all glomeruli in the regions were assessed. We eliminated

glomeruli that were inappropriate for the evaluation of glomerular sizes and/or mesangial matrix areas if they were sectioned at their vascular poles or artificially compressed or distorted. Finally, 15 images (×800 magnification) of glomeruli were obtained randomly from each superficial and juxtamedullary cortical region of individual mice. The decision for selecting glomeruli for the analysis was made blindly by an experienced clinicopathologist. Glomerular areas and PAS-positive, nucleus-free areas in the mesangium (defined as mesangial matrix areas) were assessed using Image-Pro Plus v.7.0. The mesangial matrix areas were expressed as percentages of the glomerular areas. The mean values of each mouse were evaluated statistically.

Preparation of IRPTCs Stably Expressing EGFP-LC3

pEGFP-C1 with a rat LC3 cDNA inserted downstream of EGFP cDNA (a generous gift from Professor Noboru Mizushima, Tokyo University, Japan)[47] was digested with *Eco*47III and *Eco*RI to excise the DNA fragment encoding EGFP-LC3. pQCXIP (TAKARA/Clontech) was digested with *Not*I, blunt-ended, digested with *Eco*RI, and ligated with the EGFP-LC3 fragment. The resulting plasmid and pKat2 (a generous gift from Professor Tetsuro Takeda, Dokkyo Medical College Koshigaya Hospital, Japan) were cotransfected into HEK293T cells to produce recombinant retroviruses using the ProFection Mammalian Transfection System (Promega). IRPTCs (a generous gift from Professor Julie R. Ingelfinger, Massachusetts General Hospital) were infected with the viruses, and infected cells were selected by culturing in DMEM, low glucose, pyruvate (Life Technologies, GIBCO), 25 mM HEPES (Life Technologies, GIBCO), 5% FCS, and 0.1 mM MEM nonessential amino acids (Life Technologies, GIBCO) with puromycin (1 mg/ml).

Analysis of (Auto)lysosome Formation in IRPTCs or in IRPTCs Expressing EGFP-LC3 Incubated with Fatty Acid–Rich or Fatty Acid–Depleted Albumin

IRPTCs or IRPTCs expressing EGFP-LC3 were cultured in the medium described above, except for puromycin, and incubated with fatty acid–rich BSA purified using anion chromatography (Life Technologies, GIBCO) or fatty acid–depleted BSA (Calbiochem, EMD Millipore) at a concentration of 1 mg/ml for 24 hours on gelatin-coated coverslips (Thermo Fisher Scientific). Then, LysoTracker Deep Red (Life Technologies, Molecular Probes), a lysosomal marker, and NucBlue Live Cell Stain (Life Technologies, Molecular Probes), a nuclear marker, were added to the culture media and incubated for 20 minutes. The cells were then fixed with a 4% paraformaldehyde phosphate buffer solution (Wako) and examined using a BZ-9000 microscope. LysoTracker-positive vacuoles and cell surface area were evaluated by using Image-Pro Plus v.7.0 in 20 cells selected at random.

Autophagy Flux Analysis

IRPTCs were cultured in the same condition described above and used for this analysis (see Supplemental Figure 5 for the detailed method).

RNA Interference of Megalin Expression in IRPTCs

Megalin expression was knocked down by transfecting IRPTCs with specific Silencer Select siRNAs (2.5 nM each of s130935 and s139036, Cat# 4390771; Life Technologies, Ambion) for 24 hours in medium without puromycin using the Lipofectamine RNAiMAX Reagent (Life Technologies, Invitrogen) according to the manufacturer's instructions. Nonspecific Silencer Negative Control #5 siRNA (Cat#AM4642; Life Technologies, Ambion) was used for negative control experiments (see Supplemental Figure 6 for the detailed method).

Real-Time RT-PCR of PDGF-B and MCP-1

IRPTCs that were cultured in DMEM, low glucose, pyruvate, 25 mM HEPES, and 0.1 mM MEM nonessential amino acids were used for megalin RNAi for 24 hours and incubated with fatty acid–rich BSA or fatty acid–depleted BSA at a concentration of 1 mg/ml for 3 hours. The cells underwent RNA purification using a GenElute Mammalian Total RNA Miniprep Kit (Sigma-Aldrich). The expression of rat PDGF-B and MCP-1 was analyzed by real-time RT-PCR using specific primers (forward: GTCGAGTCGGAAAGCTCATC; reverse: ACACCTCTGTACGCGTCTTG; and forward: TCTCTTCCTCCACCACTATGCAG; reverse: CTTGTAGTTCTCCAGCCGACTCA, respectively). The expression of β-actin mRNA was also measured as an internal control using the following primers (forward: GCAGTACAACCTTCTTGCAGC; reverse: CATACCCACCATCACACCC). Quantitative PCR was performed using the Thermal Cycler Dice Real Time System II (Takara) and a One Step SYBR PrimeScript PLUS RT-PCR Kit (Takara). The PCR reactions were initiated with reverse transcription at 42°C for 5 minutes, heat inactivation of reverse transcription at 95°C for 10 seconds, denaturation at 95°C for 10 seconds, followed by amplification with 45 cycles at 95°C for 5 seconds, annealing at 55°C for 30 seconds, and dissociation. Data were evaluated with Multiplate RQ software.

Statistical Analyses

The results of animal experiments were analyzed for two-factor (diet-genotype) interactions by two-way ANOVA or two-way analysis of covariance and comparisons between two groups were made by *t* test (two-tailed) using SAS Studio 3.1 (SAS Institute, Inc.), Predictive Analytics SoftWare Statistics 18 (SPSS, Inc.) and R version 3.1.2 (R Foundation for Statistical Computing). The level of significance was $P<0.05$.

ACKNOWLEDGMENTS

We thank Professors Thomas Willnow, Noboru Mizushima, Tetsuro Takeda, and Julie R. Ingelfinger for their generous gifts of the experimental materials described in the Concise Methods, and Ms. Nanako Sugita, Ms. Akiko Seino, Mr. Koichi Okuda, Mr. Kazumasa Sato, Dr. Naofumi Imai, and Dr. Taiji Matsusaka for their technical assistance.

This work was supported by Grants-in-Aid for Scientific Research from the Ministry of Education, Culture, Sports, Science, and Technology of Japan (21591023 and 26461216), and a grant for research "Development of fundamental technology for analysis and evaluation of functional agricultural products and functional foods" from the Ministry of Agriculture, Forestry, and Fisheries of Japan to A.S. (51001), and a Grant-in-Aid for Young Scientists (B) from the Ministry of Education, Culture, Sports, Science, and Technology of Japan to D.N. (23790299).

An abstract of this research was presented at the meeting of the American Society of Nephrology in Atlanta, Georgia, 2013.

DISCLOSURES

None.

REFERENCES

1. Finucane MM, Stevens GA, Cowan MJ, Danaei G, Lin JK, Paciorek CJ, Singh GM, Gutierrez HR, Lu Y, Bahalim AN, Farzadfar F, Riley LM, Ezzati M; Global Burden of Metabolic Risk Factors of Chronic Diseases Collaborating Group (Body Mass Index): National, regional, and global trends in body-mass index since 1980: systematic analysis of health examination surveys and epidemiological studies with 960 country-years and 9·1 million participants. *Lancet* 377: 557–567, 2011
2. Cerezo C, Segura J, Praga M, Ruilope LM: Guidelines updates in the treatment of obesity or metabolic syndrome and hypertension. *Curr Hypertens Rep* 15: 196–203, 2013
3. Stenvinkel P, Zoccali C, Ikizler TA: Obesity in CKD – what should nephrologists know? *J Am Soc Nephrol* 24: 1727–1736, 2013
4. Kambham N, Markowitz GS, Valeri AM, Lin J, D'Agati VD: Obesity-related glomerulopathy: an emerging epidemic. *Kidney Int* 59: 1498–1509, 2001
5. Praga M, Hernández E, Morales E, Campos AP, Valero MA, Martínez MA, León M: Clinical features and long-term outcome of obesity-associated focal segmental glomerulosclerosis. *Nephrol Dial Transplant* 16: 1790–1798, 2001
6. Saito A, Pietromonaco S, Loo AK, Farquhar MG: Complete cloning and sequencing of rat gp330/"megalin," a distinctive member of the low density lipoprotein receptor gene family. *Proc Natl Acad Sci USA* 91: 9725–9729, 1994
7. Christensen EI, Nielsen S, Moestrup SK, Borre C, Maunsbach AB, de Heer E, Ronco P, Hammond TG, Verroust P: Segmental distribution of the endocytosis receptor gp330 in renal proximal tubules. *Eur J Cell Biol* 66: 349–364, 1995
8. Biemesderfer D: Regulated intramembrane proteolysis of megalin: linking urinary protein and gene regulation in proximal tubule? *Kidney Int* 69: 1717–1721, 2006
9. Shah M, Baterina OY Jr, Taupin V, Farquhar MG: ARH directs megalin to the endocytic recycling compartment to regulate its proteolysis and gene expression. *J Cell Biol* 202: 113–127, 2013
10. Saito A, Sato H, Iino N, Takeda T: Molecular mechanisms of receptor-mediated endocytosis in the renal proximal tubular epithelium. *J Biomed Biotechnol* 2010: 403272, 2010
11. Leheste JR, Melsen F, Wellner M, Jansen P, Schlichting U, Renner-Müller I, Andreassen TT, Wolf E, Bachmann S, Nykjaer A, Willnow TE: Hypocalcemia and osteopathy in mice with kidney-specific megalin gene defect. *FASEB J* 17: 247–249, 2003
12. Weyer K, Storm T, Shan J, Vainio S, Kozyraki R, Verroust PJ, Christensen EI, Nielsen R: Mouse model of proximal tubule endocytic dysfunction. *Nephrol Dial Transplant* 26: 3446–3451, 2011
13. Kantarci S, Al-Gazali L, Hill RS, Donnai D, Black GC, Bieth E, Chassaing N, Lacombe D, Devriendt K, Teebi A, Loscertales M, Robson C, Liu T, MacLaughlin DT, Noonan KM, Russell MK, Walsh CA, Donahoe PK, Pober BR: Mutations in LRP2, which encodes the multiligand receptor megalin, cause Donnai-Barrow and facio-oculo-acoustico-renal syndromes. *Nat Genet* 39: 957–959, 2007
14. Weinberg JM: Lipotoxicity. *Kidney Int* 70: 1560–1566, 2006
15. Thomas MC: Advanced glycation end products. *Contrib Nephrol* 170: 66–74, 2011
16. Deji N, Kume S, Araki S, Soumura M, Sugimoto T, Isshiki K, Chin-Kanasaki M, Sakaguchi M, Koya D, Haneda M, Kashiwagi A, Uzu T: Structural and functional changes in the kidneys of high-fat diet-induced obese mice. *Am J Physiol Renal Physiol* 296: F118–F126, 2009
17. Tojo A, Sekine T, Nakajima N, Hosoyamada M, Kanai Y, Kimura K, Endou H: Immunohistochemical localization of multispecific renal organic anion transporter 1 in rat kidney. *J Am Soc Nephrol* 10: 464–471, 1999
18. Yamahara K, Kume S, Koya D, Tanaka Y, Morita Y, Chin-Kanasaki M, Araki H, Isshiki K, Araki S, Haneda M, Matsusaka T, Kashiwagi A, Maegawa H, Uzu T: Obesity-mediated autophagy insufficiency exacerbates proteinuria-induced tubulointerstitial lesions. *J Am Soc Nephrol* 24: 1769–1781, 2013
19. Cao X, Xue L, Han L, Ma L, Chen T, Tong T: WW domain-containing E3 ubiquitin protein ligase 1 (WWP1) delays cellular senescence by promoting p27(Kip1) degradation in human diploid fibroblasts. *J Biol Chem* 286: 33447–33456, 2011
20. Gahan PB: Histochemistry of lysosomes. *Int Rev Cytol* 21: 1–63, 1967
21. Declèves AE, Zolkipli Z, Satriano J, Wang L, Nakayama T, Rogac M, Le TP, Nortier JL, Farquhar MG, Naviaux RK, Sharma K: Regulation of lipid accumulation by AMP-activated kinase [corrected] in high fat diet-induced kidney injury. *Kidney Int* 85: 611–623, 2014
22. Panossian L, Fenik P, Zhu Y, Zhan G, McBurney MW, Veasey S: SIRT1 regulation of wakefulness and senescence-like phenotype in wake neurons. *J Neurosci* 31: 4025–4036, 2011
23. Schönenbrücher H, Adhikary R, Mukherjee P, Casey TA, Rasmussen MA, Maistrovich FD, Hamir AN, Kehrli ME Jr, Richt JA, Petrich JW: Fluorescence-based method, exploiting lipofuscin, for real-time detection of central nervous system tissues on bovine carcasses. *J Agric Food Chem* 56: 6220–6226, 2008
24. Negre-Salvayre A, Auge N, Ayala V, Basaga H, Boada J, Brenke R, Chapple S, Cohen G, Feher J, Grune T, Lengyel G, Mann GE, Pamplona R, Poli G, Portero-Otin M, Riahi Y, Salvayre R, Sasson S, Serrano J, Shamni O, Siems W, Siow RC, Wiswedel I, Zarkovic K, Zarkovic N: Pathological aspects of lipid peroxidation. *Free Radic Res* 44: 1125–1171, 2010
25. Itakura K, Oya-Ito T, Osawa T, Yamada S, Toyokuni S, Shibata N, Kobayashi M, Uchida K: Detection of lipofuscin-like fluorophore in oxidized human low-density lipoprotein. 4-hydroxy-2-nonenal as a potential source of fluorescent chromophore. *FEBS Lett* 473: 249–253, 2000
26. Kerjaschki D, Exner M, Ullrich R, Susani M, Curtiss LK, Witztum JL, Farquhar MG, Orlando RA: Pathogenic antibodies inhibit the binding of apolipoproteins to megalin/gp330 in passive Heymann nephritis. *J Clin Invest* 100: 2303–2309, 1997
27. Hall AM, Rhodes GJ, Sandoval RM, Corridon PR, Molitoris BA: In vivo multiphoton imaging of mitochondrial structure and function during acute kidney injury. *Kidney Int* 83: 72–83, 2013
28. Nishioka S, Nakano D, Kitada K, Sofue T, Ohsaki H, Moriwaki K, Hara T, Ohmori K, Kohno M, Nishiyama A: The cyclin-dependent kinase inhibitor p21 is essential for the beneficial effects of renal ischemic preconditioning on renal ischemia/reperfusion injury in mice. *Kidney Int* 85: 871–879, 2014
29. Schrimpf C, Duffield JS: Mechanisms of fibrosis: the role of the pericyte. *Curr Opin Nephrol Hypertens* 20: 297–305, 2011
30. Lin SL, Chang FC, Schrimpf C, Chen YT, Wu CF, Wu VC, Chiang WC, Kuhnert F, Kuo CJ, Chen YM, Wu KD, Tsai TJ, Duffield JS: Targeting endothelium-pericyte cross talk by inhibiting VEGF receptor signaling attenuates kidney microvascular rarefaction and fibrosis. *Am J Pathol* 178: 911–923, 2011
31. Chen YT, Chang FC, Wu CF, Chou YH, Hsu HL, Chiang WC, Shen J, Chen YM, Wu KD, Tsai TJ, Duffield JS, Lin SL: Platelet-derived growth factor receptor signaling activates pericyte-myofibroblast transition in obstructive and post-ischemic kidney fibrosis. *Kidney Int* 80: 1170–1181, 2011
32. Fredriksson L, Li H, Eriksson U: The PDGF family: four gene products form five dimeric isoforms. *Cytokine Growth Factor Rev* 15: 197–204, 2004
33. Tang WW, Ulich TR, Lacey DL, Hill DC, Qi M, Kaufman SA, Van GY, Tarpley JE, Yee JS: Platelet-derived growth factor-BB induces renal tubulointerstitial myofibroblast formation and tubulointerstitial fibrosis. *Am J Pathol* 148: 1169–1180, 1996

34. Motoyoshi Y, Matsusaka T, Saito A, Pastan I, Willnow TE, Mizutani S, Ichikawa I: Megalin contributes to the early injury of proximal tubule cells during nonselective proteinuria. *Kidney Int* 74: 1262–1269, 2008
35. Theilig F, Kriz W, Jerichow T, Schrade P, Hähnel B, Willnow T, Le Hir M, Bachmann S: Abrogation of protein uptake through megalin-deficient proximal tubules does not safeguard against tubulointerstitial injury. *J Am Soc Nephrol* 18: 1824–1834, 2007
36. Jiang M, Liu K, Luo J, Dong Z: Autophagy is a renoprotective mechanism during in vitro hypoxia and in vivo ischemia-reperfusion injury. *Am J Pathol* 176: 1181–1192, 2010
37. Kimura T, Takabatake Y, Takahashi A, Kaimori JY, Matsui I, Namba T, Kitamura H, Niimura F, Matsusaka T, Soga T, Rakugi H, Isaka Y: Autophagy protects the proximal tubule from degeneration and acute ischemic injury. *J Am Soc Nephrol* 22: 902–913, 2011
38. Jiang M, Wei Q, Dong G, Komatsu M, Su Y, Dong Z: Autophagy in proximal tubules protects against acute kidney injury. *Kidney Int* 82: 1271–1283, 2012
39. Liu D, Wen Y, Tang TT, Lv LL, Tang RN, Liu H, Ma KL, Crowley SD, Liu BC: Megalin/cubulin-lysosome-mediated albumin reabsorption is involved in the tubular cell activation of NLRP3 inflammasome and tubulointerstitial inflammation. *J Biol Chem* 290: 18018–18028, 2015
40. Madsen KM, Park CH: Lysosome distribution and cathepsin B and L activity along the rabbit proximal tubule. *Am J Physiol* 253: F1290–F1301, 1987
41. Ivy GO, Roopsingh R, Kanai S, Ohta M, Sato Y, Kitani K: Leupeptin causes an accumulation of lipofuscin-like substances and other signs of aging in kidneys of young rats: further evidence for the protease inhibitor model of aging. *Ann N Y Acad Sci* 786: 12–23, 1996
42. Reisman SA, Chertow GM, Hebbar S, Vaziri ND, Ward KW, Meyer CJ: Bardoxolone methyl decreases megalin and activates nrf2 in the kidney. *J Am Soc Nephrol* 23: 1663–1673, 2012
43. Pergola PE, Raskin P, Toto RD, Meyer CJ, Huff JW, Grossman EB, Krauth M, Ruiz S, Audhya P, Christ-Schmidt H, Wittes J, Warnock DG; BEAM Study Investigators: Bardoxolone methyl and kidney function in CKD with type 2 diabetes. *N Engl J Med* 365: 327–336, 2011
44. Tsuboi N, Utsunomiya Y, Kanzaki G, Koike K, Ikegami M, Kawamura T, Hosoya T: Low glomerular density with glomerulomegaly in obesity-related glomerulopathy. *Clin J Am Soc Nephrol* 7: 735–741, 2012
45. Hosaka K, Takeda T, Iino N, Hosojima M, Sato H, Kaseda R, Yamamoto K, Kobayashi A, Gejyo F, Saito A: Megalin and nonmuscle myosin heavy chain IIA interact with the adaptor protein Disabled-2 in proximal tubule cells. *Kidney Int* 75: 1308–1315, 2009
46. Nakano D, Doi K, Kitamura H, Kuwabara T, Mori K, Mukoyama M, Nishiyama: A reduction of tubular flow rate as a mechanism of oliguria in the early phase of endotoxemia revealed by intravital imaging [published online ahead of print April 8, 2015]. *J Am Soc Nephrol* doi: 10.1681/ASN.2014060577
47. Bampton ET, Goemans CG, Niranjan D, Mizushima N, Tolkovsky AM: The dynamics of autophagy visualized in live cells: from autophagosome formation to fusion with endo/lysosomes. *Autophagy* 1: 23–36, 2005

This article contains supplemental material online at http://jasn.asnjournals.org/lookup/suppl/doi:10.1681/ASN.2015020190/-/DCSupplemental.